

CO LUMINOSITY FUNCTIONS FOR FIR AND B-BAND SELECTED GALAXIES AND THE FIRST ESTIMATE FOR Ω_{HI+H_2}

DUSAN KERES, MIN S. YUN & J. S. YOUNG

Department of Astronomy, University of Massachusetts, Amherst, MA 01003
keres@nova.astro.umass.edu, myun@astro.umass.edu, young@astro.umass.edu
To appear in The Astrophysical Journal

ABSTRACT

We derive a non-parametric CO luminosity function using a FIR and an optical *B*-band selected sample of the galaxies included in the FCRAO Extragalactic CO Survey. The FIR selected sample is defined using the IRAS Bright Galaxy Surveys (BGS; IRAS 60 micron flux density ≥ 5.24 Jy). Although our CO sample is not complete, the normalization using the BGS reproduces the IRAS 60 micron luminosity function in excellent agreement with those found in the literature. Similarly, a *B*-band selected sample defined using the Revised Shapley-Ames (RSA) catalog is used to derive a CO luminosity function for a comparison. A Schechter function describes the both derived CO luminosity functions reasonably well. Adopting the standard CO-to- H_2 conversion factor, we derive a molecular gas density of $\rho_{H_2} = (3.1 \pm 1.2) \times 10^7 h M_\odot \text{ Mpc}^{-3}$ for the local volume. Combining with the measurements of the local HI mass density and the helium contribution, we estimate that the total mass density of cold neutral gas in the local universe is $\Omega_{gas} = (4.3 \pm 1.1) \times 10^{-4} h^{-1}$, which is about 20% of the total stellar mass density Ω_* .

Subject headings: galaxies: luminosity function – galaxies: ISM – galaxies: surveys – ISM: molecules – radio lines: ISM – cosmology: cosmological parameters

1. INTRODUCTION

The star formation history of the Universe is closely linked with the evolution of the gas content of the Universe. Observations of the distribution and total gas content in galaxies and in intergalactic clouds offer some of the most important observational constraints for the cosmology and galaxy evolution models. Because stars form out of cold, dense gas clouds, the history of galaxy formation and evolution is also the history of gas accretion and conversion into stars. Here we derive the total cold gas density for the local volume by deriving the local CO luminosity function and combining with the existing estimates of the neutral atomic gas density.

A variety of luminosity functions (LFs) and mass functions are found in the literature: optical (e.g. Marzke, Huchra, & Geller 1994), HI (e.g. Zwaan et al. 1997; Schneider et. al 1998), and infrared (e.g. Soifer et al. 1987; Yun et al. 2001). While several groups have investigated the local neutral hydrogen density, little information is available on the molecular gas content in galaxies because of the lack of appropriate data. In her pioneer work, Verter (1987) derived averaged values of CO luminosity and the CO/HI flux ratio based on a maximum likelihood probability distribution for 40 galaxies and 47 upper limits obtained by combining all available data at the time. Since the large fraction of the CO measurements used were non-detections (upper limits), the derivation of the CO luminosity function was highly problematic. Nevertheless, a general trend of increasing number of CO emitting galaxies per unit volume with decreasing CO luminosity was suggested by this analysis.

Nearly 15 years later, the availability of the extragalactic CO data has improved greatly. The FCRAO (Five College Radio Astronomy Observatory) Extragalactic CO Survey

(Young et al. 1995) represents a particularly rich database for the investigation of CO luminosity function and molecular gas content in galaxies. We have constructed a large, statistically significant sample of far-infrared (FIR) and optical *B*-band selected galaxies from this survey and derived a non-parametric CO luminosity function. Our sample galaxies range over 4 orders of magnitudes in CO luminosity, and only a small fraction are non-detections. Since CO is a tracer of hydrogen molecules, molecular hydrogen mass can be derived from CO luminosity. By integrating the resulting molecular gas mass function, we then derive the molecular gas mass density and the total cold gas mass density of the local universe.

2. SAMPLE SELECTION AND PROPERTIES

The FCRAO Extragalactic CO Survey (“the Survey”, herein) is the largest CO survey of galaxies available in the literature, containing observations of 300 galaxies at 1421 positions (Young et al. 1995). Since the Survey covers a broad range of Hubble types and contains a large number of detections (236 or 79%), it is well suited for a statistical analysis and for constructing a CO luminosity function. The majority of the survey galaxies were selected from the Second Reference Catalog (RC2; de Vaucouleurs et. al 1976) or the IRAS database. Most of the galaxies in the Survey are spiral or irregular galaxies at declination north of -25° and satisfy at least one of the following three criteria: $B_T^0 < 13$, $S_{60\mu m} > 5$ Jy, or $S_{100\mu m} > 10$ Jy (see Young et al. 1995, for a detailed description). The majority of the detected galaxies in the Survey were observed at multiple positions along the major axis, and the total CO fluxes were derived by modeling the underlying CO distribution.

The Survey is not complete in terms of any of the sample selection criteria, and the full sample cannot be used directly for a statistical analysis in a straightforward way. The analysis of the velocity integrated CO luminosity is further complicated by the fact that the CO line width varies from one galaxy to another (and even one position to another in a given galaxy) while the sensitivity achieved also varies depending on the observing condition even if identical integration times are used (typically 2-4 hours). Therefore, it is difficult to address the sensitivity and completeness limit of the Survey in terms of the observed CO flux. Instead, taking advantage of the well-known tight correlation between the FIR and CO luminosity (see Young et al. 1995), we utilize the IRAS 60 μm flux density of the individual sample galaxies to define a complete sample for a statistical analysis and the derivation of the CO LF. We further test the robustness of the technique and the selection bias by deriving the CO luminosity function using the optical B -band selection (see § 3.3). Previously Briggs & Rao (1993) successfully derived the HI mass function for the field galaxies using the optical selection, and the radio luminosity function has been successfully derived using the FIR selection function by Yun et al. (2001).

Taking advantage of the well defined and well studied IRAS Bright Galaxy Samples (BGSs; Soifer et al. 1989; Sanders et al. 1995), we adopt the sample selection criterion of 60 μm flux density limit greater than 5.24 Jy. A total of 200 galaxies in the Survey satisfy this criteria. Most of the selected galaxies are spirals of types Sa-Sc while 14 galaxies are mergers, 7 galaxies are close pairs, and 3 galaxies have no type determined. In most cases we adopt the 60 μm fluxes from the BGS surveys. For galaxies with angular diameters larger than 8', we adopt the values from Rice et al. (1988) after multiplying by 1.18 in order to match the flux scaling (see Devereux & Young 1990). This rescaling has little impact on our sample completeness limit because most of our sample galaxies have flux densities much larger than 5.24 Jy. Some of the 60 μm flux density measurements come from Young et al. (1989, 2002), and 10 galaxies satisfying our selection criterion are added to the sample. Five of these galaxies are not in the BGS survey area, and two are present in Rice et al. (1988) but not in the BGS surveys.

There are 12 galaxies in our selected sample that are brighter than 5.24 Jy at 60 μm and were not detected in CO (see Table 1). The CO (1-0) flux measurements for five of these galaxies are found in the literature. The remaining 7 galaxies are treated as two limiting cases: (a) as detections with zero flux; and (b) as detections at the upper limit flux value (see Verter 1987). A large number of non-detections would severely limit the determination of the true CO LF, but the non-detections account for less than 4% in our sample and thus have little overall impact.

Some of the galaxy distances come from direct measurements such as using Cepheids. We adopt a Hubble constant of $H_0 = 75 \text{ km s}^{-1} \text{ Mpc}^{-1}$ for the remaining galaxies. Since we are using the CO database obtained from largely a single instrument (2.5% of the sample taken from other surveys), the internal consistency of the data and the analysis should be quite good. Our sample also includes 26

galaxies in the Virgo cluster. We adopt a uniform distance of 16 Mpc for the Virgo galaxies. We have constructed a CO LF with and without Virgo galaxies in order to see if the presence of the cluster galaxies influenced the shape of the CO LF (see § 3).

To examine the uniformity and completeness of our sample, we have analyzed the differential number count statistics as a function of the 60 μm flux density (see Fig. 1). If the 60 μm sources are uniformly distributed in a Euclidean space and are not evolving, the resulting differential number count should be a power-law distribution with $N \propto S^{-3/2}$. The number of sample galaxies per bin shown in Figure 1 is consistent with such a power-law, but the slope is somewhat shallower. When all of the flux density bins are included, the best fit power-law index is $\alpha = -1.0$, where $\log N = N_0 + \alpha \times \log S$. For the 60 μm flux density between 10 and 100 Jy where most of the sample galaxies fall, the differential number counts are more consistent with the uniform distribution within the statistical uncertainties.

There are several factors contributing to the flatter than expected power-law slope in the observed number counts in Figure 1. First of all, the spatial distribution of galaxies is in general *not* uniform, particularly given the relatively high flux density cutoff we adopted. The situation is exacerbated by the fact that our Galaxy is located within a galaxy aggregate called the Local Supercluster. The flattening of the galaxy counts among the high flux density bins as seen in Figure 1 is an immediate outcome of the local large scale structures. Soifer et al. (1989) noted a similar number count enhancement in their analysis of the first Bright Galaxy Sample (BGS1). The mean $\langle V/V_m \rangle$ for our sample is about 0.35, indicating that on average our sample galaxies are about 10% closer than the uniform case. The $\langle V/V_m \rangle$ values are particularly low for the $\log L_{60\mu\text{m}}$ bins of 9.6-10.4 (see Fig. 2), and similar trend is also seen in the $\langle V/V_m \rangle$ plot by Soifer et al. (1989). Comparison to Soifer et al. (1989) value $\langle V/V_m \rangle = 0.47$ is suggesting that major cause of this discrepancy is weak bias in our sample towards galaxies closer than average expected from the complete sample, while the large scale structure plays less important role. Although the FCRAO CO Survey selected target galaxies ‘‘at random’’ from the parent sample of IRAS and B -band selected galaxies, a slight bias favoring galaxies which were well suited to the FCRAO resolution (1'-5' in size) is also present. Such a bias manifests non-trivially in these statistics, however. Given the limitation of our sample, such as selecting galaxies suitable for observation with FCRAO telescope and the local large scale structures, the steep power-law index of $\alpha \sim -1.2$ shown in Figure 1 suggests that our assumption of random and uniform sampling from the parent samples still seems reasonable. Effects of these potential biases on the derivation of the LFs are evaluated by the derivation of the 60 μm LF using the same sample, as discussed below.

3. LUMINOSITY FUNCTIONS

A luminosity function represents the space density of the sample galaxies per luminosity bin (ΔL) centered on L . It represents the probability density of finding a galaxy with a specific luminosity, and it also contains information

on the total luminosity in the sampled volume. We use the classical $1/V_m$ method (Schmidt 1968) to derive the LF and associated uncertainty directly as:

$$\rho(L) = \sum_{i=1}^N \frac{1}{V_m^i}, \quad \sigma_\rho(L) = \left(\sum_{i=1}^N \frac{1}{(V_m^i)^2} \right)^{1/2} \quad (1)$$

where $\rho(L)$ is number of objects per volume per luminosity bin centered on luminosity L , V_m is the sample volume appropriate for each of the galaxies, and N is the number of galaxies in the bin.

The FCRAO Extragalactic CO Survey covers the same area as the IRAS BGS (Soifer et al. 1989; Sanders et al. 1995), and we selected a subset using the same IRAS 60 μm flux density cutoff. Therefore, the sampling correction for our sample can be reduced to a simple scaling relation if our sample is a fair subset of the BGS, as argued above (§ 2). In this case, the scaling factor is the ratio of the number of galaxies contained in BGS surveys and number of galaxies in our sample.

The sample volume obtained using this approach is:

$$V_m = \Omega \frac{N_{FCRAO}}{N_{BGS}} \frac{D^3}{3} = 1.16 \times D^3 \quad (2)$$

where D is maximum distance at which galaxy of given luminosity could be detected for a given flux limit, and Ω is the total solid angle covered by both BGS1 (Soifer et al. 1989) and BGS2 (Sanders et al. 1995) in *steradian*. N_{FCRAO}/N_{BGS} is the ratio of the number of galaxies in our sample and the number of galaxies in both BGS samples. BGS1 and BGS2 together contain 601 galaxies and cover 83% of the sky.

3.1. 60 μm Luminosity Function

The 60 μm luminosity represents the contribution from the IRAS 60 μm band to the FIR luminosity (Helou et al. 1988) and was calculated using the following relation from Yun et al. (2001) :

$$\log L_{60\mu\text{m}}(L_\odot) = 6.014 + 2\log D + \log S_{60\mu\text{m}} \quad (3)$$

where D is the distance in Mpc and $S_{60\mu\text{m}}$ is the IRAS 60 μm band flux density in Jy.

As a way to verify our CO sample correction and to evaluate the effects of various sample biases discussed in § 2, we first derive the 60 μm LF for our CO-selected galaxies in order to compare it to the previously published 60 μm LF by Yun et al. (2001). As shown on Figure 3, the agreement between the two 60 μm luminosity functions is excellent. Yun et al. sample was selected with 2.5 times smaller flux density cutoff than the BGS and is thus 9 times larger in size. While this is not a complete verification of our derivation method, this agreement lends support to our assumption that our sample is a fair subset of the complete 60 μm selected sample. The normalization factor could in principle be dependent on the 60 μm luminosity. The comparison of the 60 μm LFs suggests that this dependence is weak if any.

About 13% of our sample are Virgo cluster galaxies. Again, the 60 μm luminosity function was constructed including and excluding Virgo galaxies. The resulting luminosity functions are very similar – see Figure 4. The similarity would arise if the cluster galaxies are distributed in

luminosity bins in the same manner as the field galaxies and if the Virgo galaxies contribute only a small fraction to each luminosity bin. Previous studies of Virgo galaxies have suggested that their molecular gas contents are affected little by their cluster environment (e.g. Kenney & Young 1989). Since we are interested in the total cold gas density of the local volume regardless of the galaxy environment, we include all Virgo galaxies in our analysis here on.

3.2. CO Luminosity Function

Encouraged by the success of deriving the 60 μm LF above for the 200 galaxies in our sample, the CO luminosity function is derived using the $^{12}\text{CO}(1-0)$ flux with the same sample and volume correction. The CO luminosity is calculated as $L_{CO} = 4\pi D^2 S_{CO}$, where D is the distance to the galaxy in Mpc and S_{CO}^1 is the velocity integrated CO flux in Jy km s^{-1} . The computed CO luminosity for our sample galaxies ranges between 10^4 and 10^8 $\text{Jy km s}^{-1} \text{Mpc}^2$. They are divided into 10 bins of unit magnitude (0.4 wide in a log scale). There are larger uncertainties at the low luminosity end because only a small number of sources occupy these bins.

The resulting CO luminosity function is shown in Figure 4. It is well described by a Schechter function which has an exponential cutoff at high luminosity end. The low luminosity end power-law slope is quite flat, similar to the 60 μm LF (see § 4). To quantify these properties, the characteristic parameters are derived for the Schechter function (Schechter 1976) of the form

$$\phi(L)d(L) = \phi^* \left(\frac{L}{L^*} \right)^\alpha \exp\left(-\frac{L}{L^*}\right) d\left(\frac{L}{L^*}\right) \quad (4)$$

where ϕ^* is the normalization factor, α is the low luminosity end power-law slope, and L^* is the characteristic luminosity at which the exponential cutoff develops. Since we are using logarithmic intervals to construct LF, we need to change this equation to an appropriate form:

$$\rho(L) = \rho^* \left(\frac{L}{L^*} \right)^{\alpha+1} \exp\left(-\frac{L}{L^*}\right) \ln 10 \quad (5)$$

in this case $\rho(L) = \phi(L)d(L)/d(\log(L))$, and it is calculated using eq. (1). The derived best fit Schechter parameters are: $\rho^* = (0.00072 \pm 0.00035) \text{Mpc}^{-3} \text{mag}^{-1}$, $\alpha = (-1.30 \pm 0.16)$, and $L^* = (1.0 \pm 0.2) \times 10^7 \text{Jy km s}^{-1} \text{Mpc}^2$ ($M^* = 9.4 \pm 1.9 \times 10^9 M_\odot$ using the standard CO-to- H_2 conversion factor – see § 4.2).

The single Schechter function fit using all 10 luminosity bins produces a rather poor fit with $\chi^2 = 50$. This poor fit is also obvious in Figure 4 as the single Schechter function fit shown with a solid line is only marginally consistent with the data points and their formal uncertainties. It is possible that a Schechter function is intrinsically a poor functional form for the CO LF. On the other hand, a Schechter function successfully describes many other LFs including the HI LF (e.g. Schneider et al. 1998). There is also a theoretical basis in that it is the functional form associated with the halo mass function in the Press-Schechter formulation of the structure formation (Press & Schechter 1974).

¹ We adopt the definition $S_{CO} \equiv \int I_{CO} d\Omega$, following the same notation as Young et al. (1995).

One possible explanation for such a large χ^2 value is that there are two (or more) distinct populations of galaxies in the sample, similar to the situation with the FIR luminosity function as noted by Yun et al. (2001). In the FIR, the light-to-mass ratio for the starburst population is systematically enhanced by 1-2 orders of magnitudes over the field population. The CO luminosity is also thought to be elevated significantly among the intense nuclear starburst systems (Scoville, Yun, & Bryant 1997; Downes & Solomon 1998), and this may materialize as two distinct populations in the CO LF as well. There are 14 mergers/starburst systems in our sample, and eight of these fall within the last two bins and account for about 40% of the galaxies in these bins. When a best fit Schechter function is derived using only the first 8 bins dominated by normal field galaxies, the χ^2 value drops to 13, which is a significant improvement. The Schechter function fit for the bins dominated by normal galaxies gives: $\rho^* = (0.003 \pm 0.001) \text{ Mpc}^{-3} \text{ mag}^{-1}$, $\alpha = (-0.90 \pm 0.15)$, and $L^* = (3.3 \pm 0.6) \times 10^6 \text{ Jy km s}^{-1} \text{ Mpc}^2$ ($M^* = 3.1 \pm 0.6 \times 10^9 M_\odot$).

The difference between all Schechter parameters for the two limiting situations of treating the non-detected galaxies as upper limits or zero detections is smaller than 2%. Such a small difference is expected since we have less than 4% upper limits in our sample. Similarly, including or excluding Virgo galaxies has only a minor impact, as discussed above (see § 3.1).

3.3. CO LF from the B-band Selected Galaxies

As an independent check of our CO LF derived using the FIR selection, we also derive a CO luminosity function using an optical B-band selected sample. The method of deriving the CO LF is similar to the method used for the infrared selected galaxies: we use the $1/V_m$ method and rescaling of the number of galaxies using a complete sample, which is the Revised Shapley-Ames (RSA) catalog by Sandage & Tammann (1981) in this case. A declination cut off of $\delta > -25^\circ$ and a Galactic longitude limit of $|b| > 10^\circ$ are adopted as part of the sample definition. This makes the total surveyed area equal to 60% of the sky. Our brightness selection criterion is $B_T \leq 12.0^{mag}$.

Accounting for different Hubble types correctly is a difficult issue. Since CO emission is generally very weak or undetected among early type galaxies, only the spiral and irregular galaxies are included in the analysis. The examination of the differential number counts for our B-band selected sample yields a power-law index $\alpha = -1.35$, suggesting a reasonably good uniformity and completeness. The mean $\langle V/V_m \rangle$ ratio for the sample is 0.33 (see Fig. 2), similar to the FIR selected sample. Although we adopt the RSA catalog as a complete sample, a few galaxies satisfying our selection criteria are missing in the RSA (see Condon 1987).

The B-band magnitudes are taken from the RSA while the CO fluxes are taken from the Survey. There are 133 galaxies in the CO Survey that satisfy the selection criteria while the parent RSA catalog galaxies satisfying the selection criteria are 252 in total. In this case, CO fluxes for 13 galaxies (10%) are upper limits. The CO luminosity function derived for this B-band selected sample is shown on the Figure 5. This LF is very similar to CO LF from

the FIR selected galaxies but with a lower characteristic luminosity L^* and a larger scatter on the low luminosity end. The lower characteristic luminosity L^* is a direct consequence of the absence of mergers in this sample. The best fit Schechter parameters for the B-band derived CO luminosity function are: $\rho^* = (0.0021 \pm 0.0009) \text{ Mpc}^{-3} \text{ mag}^{-1}$, $\alpha = (-1.0 \pm 0.2)$, and $L^* = (4.8 \pm 1.1) \times 10^6 \text{ Jy km s}^{-1} \text{ Mpc}^2$ ($M^* = 4.5 \pm 1.0 \times 10^9 M_\odot$).

4. DISCUSSION

4.1. Uncertainties and biases in the CO LF

One major source of uncertainty in the derived CO luminosity function is that it is derived indirectly using the FIR and optical B-band selection functions. A direct derivation from the observed CO properties is possible in principle, but the complication associated with the *a priori* unknown line widths adds a significant uncertainty. Instead we take advantage of the known tight correlation between FIR and CO luminosity in deriving the CO LF for our sample. The 1.4 GHz radio luminosity function derived by Yun et al. (2001) using the radio-FIR correlation and IRAS 60 μm flux density agrees very well with the radio LFs derived directly (Condon, Anderson, & Helou 1991; Condon et al. 2002), giving some assurance to this technique. We have examined whether any systematic trends (thus a bias) exist in the $S_{60\mu\text{m}}/S_{\text{CO}}$ ratio as a function of the 60 μm flux density and luminosity. As shown in Figure 6, little trend is seen in this ratio, and the known linear correlation seems to hold well within the uncertainties for the entire range of flux density and luminosity.

Deriving a luminosity function for one wavelength using a selection function at another wavelength may be robust enough to work even if the two quantities are correlated in a non-linear way. There is a known correlation between FIR, CO, and optical B-band luminosity for late type galaxies, but the correlations involving the B-band luminosity are shown to be non-linear (see Young et al. 1989; Perea et al. 1997). Yet, the CO luminosity function derived using the FIR selection function (Figure 4) is in excellent agreement with the CO LF derived using the B-band selection function (Figure 5). The selection bias is present as some of the most CO luminous galaxies (merger starbursts) are missed in the B-band selected sample. Nevertheless the agreement is striking given the non-linear dependence between CO and B-band luminosity.

Another source of a significant uncertainty is the uniformity of sampling and correctly accounting for the selection function for the sample of galaxies which is not complete by the adopted selection criteria. Both the differential source count and the $\langle V/V_m \rangle$ analysis suggest a non-uniform distribution of the sample galaxies (see § 2), and a slight bias towards galaxies brighter at 60 μm may be responsible for this effect. The large scale structure also have influence in lowering $\langle V/V_m \rangle$ value for our sample. The non-trivial nature of these effects are demonstrated by the fact that including and excluding Virgo cluster galaxies from the sample make little difference to the differential source count and the $\langle V/V_m \rangle$ values.

4.2. Local Cold Gas Mass Density

CO emission is a commonly used tracer of molecular hydrogen because CO is one of the most abundant molecules in cold ISM and because its excitation in astrophysical conditions is determined by collisions with hydrogen molecules. Using the CO LF derived above, we can for the first time estimate the total mass density of molecular gas in the local volume. Adopting $N(H_2)/I(CO) = 3 \times 10^{20} \text{ cm}^{-2} [\text{K km s}^{-1}]^{-1}$ (see review by Young & Scoville 1991),

$$M(H_2) = 1.18 \times 10^4 S_{CO} D^2 M_{\odot} \quad (6)$$

where S_{CO} is total CO flux of a galaxy in Jy km s^{-1} and D is luminosity distance in Mpc.

The molecular mass density in the local volume contributed by each luminosity bin is shown in Figure 7. The dominant contribution to the mass density comes from galaxies around L^* as expected. The summation over the 10 bins gives $\rho_{H_2} = \sum M_{H_2}/V_m = (2.4 \pm 0.7) \times 10^7 M_{\odot} \text{ Mpc}^{-3}$. Integration of the LF using the Schechter parameters obtained in previous section gives a little bit smaller values: $\rho_{H_2} = (2.2 \pm 1.1) \times 10^7 M_{\odot} \text{ Mpc}^{-3}$ for the fit trough all 10 bins, and $\rho_{H_2} = (2.2 \pm 0.9) \times 10^7 M_{\odot} \text{ Mpc}^{-3}$ for fit trough first 8 bins. The second fit is more realistic, since it fits much better bins that dominate contribution to the total mass, i.e. bins around L^* . The uncertainty stated is $\pm 1\sigma$. The systematic uncertainty, which includes uncertainties in the flux measurements, distance determinations, and CO-to- H_2 conversion, is probably larger. Unless otherwise is stated, we adopt $\rho_{H_2} = (2.3 \pm 0.9) \times 10^7 M_{\odot} \text{ Mpc}^{-3}$ as an average value between values obtained from the fit and the direct summation. Since the dependence of the gas mass density on the Hubble constant ($h \equiv H_0/100 [\text{km s}^{-1} \text{ Mpc}^{-1}]^{-1}$) is linear, this result can be written as $\rho_{H_2} = (3.1 \pm 1.2) \times 10^7 h M_{\odot} \text{ Mpc}^{-3}$.

The molecular hydrogen mass density in the local volume obtained from the B -band selected sample is $\rho_{H_2} = (3.1 \pm 0.9) \times 10^7 h M_{\odot} \text{ Mpc}^{-3}$ using a direct summation of the contribution of each galaxy and $(3.1 \pm 1.5) \times 10^7 h M_{\odot} \text{ Mpc}^{-3}$ using the best fit Schechter parameters. Values for the local molecular mass density obtained from the FIR selected sample and the B -band selected sample are in good agreement. Since we have better statistics for the larger FIR selected sample, we adopt the local molecular gas mass density derived from the FIR selected sample here on. Using observed H_2 /HI mass ratio for different morphological types of galaxies and fraction of each morphological type Fukugita et al. (1998) estimated a similar value for ρ_{H_2} .

In comparison, Zwaan et al. (1997) estimated the local atomic gas mass density of $\rho_{HI} = (5.8 \pm 1.2) \times 10^7 h M_{\odot} \text{ Mpc}^{-3}$ from their Arecibo HI strip survey while Rao & Briggs (1993) derived $\rho_{HI} = (4.8 \pm 1.1) \times 10^7 h M_{\odot} \text{ Mpc}^{-3}$ from a sample of optically selected galaxies. Therefore, the molecular gas mass density in the local volume is about 50-65% of the atomic mass density, and molecular gas represents a significant component of the total mass density of the neutral gas. The HI masses for 176 galaxies in our sample are known (Young et al. 1995), and we have computed the HI mass density in the local volume using the same procedure as for the H_2 mass density. A summation over the HI mass weighted by V_m gives a value consistent with the value obtain by Zwaan et al. (1997).

We examined our sample for any trends in M_{H_2}/M_{HI} ratio vs. M_{HI} and M_{H_2} . For the range of HI masses,

$8.8 < \log M_{HI}(M_{\odot}) < 11$, the ratio of molecular to neutral atomic hydrogen masses is on average around unity with considerable scatter (see Fig. 8a). Masked in the large scatter is a possible trend in M_{H_2}/M_{HI} as a function of Hubble type (see Young et al. 1989). A clearer trend of increased M_{H_2}/M_{HI} ratio with increasing H_2 mass is seen in Figure 8b. For $\log M_{H_2}(M_{\odot}) < 8.5$, the average of this ratio is below 0.5 while the ratio jumps to around 2 near $M_{H_2} \sim 10^9 M_{\odot}$. Above H_2 mass of $10^9 M_{\odot}$, on average galaxies have more molecular than atomic gas.

Using the molecular gas mass density derived here and the value of HI mass density from Zwaan et al. (1997) we derive a total cold gas mass density at present epoch as a fraction of the critical density $\Omega_{HI+H_2} = (3.2 \pm 0.8) \times 10^{-4} h^{-1}$. Supposing that He contributes 25% of the total gas mass density, we add 33% to the derived value of Ω_{HI} , which gives $\Omega_{HI+H_2+He} \equiv \Omega_{gas} = (4.3 \pm 1.1) \times 10^{-4} h^{-1}$. These values for total neutral gas mass density are 15% smaller if we use Rao & Briggs (1993) value for the HI mass density.

The present baryon density estimated from the D/H ratio and Big Bang nucleosynthesis is $\Omega_b = 0.02 \pm 0.002 h^{-2}$ (Burles et al. 2001) while the estimate from the cosmic microwave background anisotropy is also around $\Omega_b \simeq 0.02 h^{-2}$ (de Bernardis et al. 2002). The stellar mass contents account for $\Omega_* \simeq 0.0025 h^{-1}$ (Cole et al. 2001; but also see Benson, Frenk, & Sharples 2002). We conclude that the cold gas content of late type galaxies is around 20% of the stellar mass content and about 2% of the total baryonic content in the current epoch.

4.3. CO-to- H_2 conversion

The lack of electric dipole moment makes direct observations of molecular hydrogen difficult in general, and studying the spatial extent and molecular gas mass requires another tracer. Highly abundant, chemically robust, and easily excited by collision with H_2 molecules, CO is the most commonly used tracer of molecular gas. The CO (1-0) transition is optically thick under most astrophysically interesting conditions, making it relatively insensitive to metallicity and abundance effects. The two key excitation parameters of density and temperature have a nearly canceling effect, making CO a fairly reliable tracer of H_2 in a broad range of physical conditions (see reviews by Maloney & Black 1988; Young & Scoville 1991).

The derived ratios of $N(H_2)/I(CO)$ range between $(1 - 5) \times 10^{20} \text{ cm}^{-2} [\text{K km s}^{-1}]^{-1}$ (Bloemen et al. 1986; Dickman et al. 1986; Scoville & Sanders 1987). We adopt a constant CO-to- H_2 conversion factor of $N(H_2)/I(CO) = 3 \times 10^{20} \text{ cm}^{-2} [\text{K km s}^{-1}]^{-1}$ (see discussions by Young & Scoville 1991). Devereux & Young (1990) show that the H_2 mass estimates of galaxies from their CO luminosity are accurate to $\pm 30\%$. Young & Scoville (1991) show that the CO-to- H_2 conversion for galaxies of diverse morphology and metallicity are similar in absolute value to the conversion in the Milky Way. While the H_2 mass estimate for an individual galaxy may be uncertain to about 30%, the H_2 mass estimate for an ensemble of galaxies should be more reliable. In most galaxies, giant molecular clouds (GMCs) and cloud complexes dominate the total molecular gas mass, and adopting a conversion factor consistent with the values derived from the Galactic GMCs

should yield the most robust, mass-weighted estimates of gas masses.

Among the low metallicity galaxies such as Small Magellanic Cloud, CO abundance may become low enough to affect the standard assumption of self-shielding and thermalization. The derived conversion factors are generally larger (e.g. Wilson 1995), and low metallicity dwarf galaxies are often undetected entirely in CO. Therefore the H_2 mass and mass density derived from the CO luminosity are strictly lower limits since molecular gas from these galaxies is missing from our analysis. On the other hand, the contribution by the low luminosity bins to our derived H_2 mass density is small (see Fig. 7) as the majority of the contribution to the total mass density comes from bins around L^* . Therefore, we can largely neglect the effect of low metallicity, low luminosity galaxies in the derivation of the total molecular gas mass density for the local volume.

As discussed already in § 3.2, the CO emission may be elevated for the FIR luminous galaxies with nuclear gas concentrations, and the CO-to- H_2 conversion factor may be smaller than the canonical value. In the extreme environment of the nuclear starburst regions, CO emission arises from a multi-phase medium with sub-thermal excitation in the diffuse phase, and the standard conversion factor may over-estimate the molecular gas mass by a factor as large as 3 to 5 (Scoville, Yun, & Bryant 1997; Downes & Solomon 1998). Such merger/starburst galaxies contribute significantly only for the top two luminosity bins in our CO LF, and these two bins contribute less than 5% to the total molecular gas mass density. Therefore, the high CO luminosity conversion factor does not have a significant impact on the derived total molecular mass density.

Similarly, increased CO emission in the central 1 kpc of our Galaxy and other galaxies has been suggested by recent observations (Paglione et. al 2001, S. Hüttemeister, private communication). High angular resolution observations of gas-rich spiral galaxies frequently reveal a distinct component in the central 1 kpc (see Sakamoto et al. 1999), and some fraction of the total CO luminosity may arise from such a component. On the other hand, among the Virgo spirals studied by Kenney & Young (1988), a simple exponential distribution without a significant central component offers a good fit for the 12 out of 14 galaxies whose CO emission is spatially well resolved (i.e., CO detected at ≥ 4 positions along the major axis). We made no attempt to account for enhanced CO emission in the central kpc as the required information is generally not available. If the molecular gas properties of Virgo spirals are typical of the late type field galaxies, then the possible contribution by the enhanced nuclear CO emission in some galaxies may not be substantial.

In summary, using the canonical CO-to- H_2 conversion relation is problematic in some cases, such as low metallicity systems or luminous nuclear starburst systems, and CO is a poor tracer of molecular gas among low metallicity dwarfs. For these reasons the local molecular gas mass density we infer is really a lower limit. However, since the majority of the mass contribution comes from L^* galaxies whose molecular gas mass is dominated by GMCs like our Galaxy, the use of the standard conversion factor still offers a fairly reliable estimate of the total molecular gas

density for the local volume.

5. SUMMARY

Utilizing the largest available CO survey, the FCRAO Extragalactic CO Survey (Young et al. 1995), the CO luminosity function for the local volume is derived using (1) a FIR selected sample of 200 galaxies that satisfy $S_{60\mu m} > 5.24 Jy$ and (2) optical B -band selected sample of 133 galaxies. Although neither of the samples is complete in terms of the sample selection, a sampling function is constructed using a well defined parent sample, and a non-parametric CO luminosity function is derived from each sample. By examining the properties of the CO luminosity functions, we conclude:

1. The CO luminosity functions derived from the FIR and B -band selected samples are reasonably well described by a Schechter function. The characteristic luminosity L^* is around $L_{CO} \sim 10^7 Jy km s^{-1} Mpc^2$. The low luminosity end of the CO luminosity function is ($\alpha = -1.3$ to -0.9). Similar values are obtained for the two CO LFs derived using the two differently selected samples.
2. The molecular gas mass density of the local volume is $\rho_{H_2} = (3.1 \pm 1.1) \times 10^7 h M_{\odot} Mpc^{-3}$ which is about 50-65% of the HI gas mass density. This value is not strongly affected by variations in the CO-to- H_2 conversion factor for low and high luminosity galaxies since it is dominated by the L^* galaxies with $L_{CO} \sim 10^7 Jy km s^{-1} Mpc^2$ ($M_{H_2}^* \sim 5 \times 10^9 M_{\odot}$). Its dependence on the global CO-to- H_2 conversion factor is linear and should be secure to within a factor of 30% or better.
3. Combined with the HI gas mass density, we estimate the total cold gas mass density at the present epoch as a fraction of the critical density $\Omega_{HI+H_2} = (3.2 \pm 0.8) \times 10^{-4} h^{-1}$. When the He contribution is included, the cold gas mass density increase to $\Omega_{HI+H_2+He} \equiv \Omega_{gas} = (4.3 \pm 1.1) \times 10^{-4} h^{-1}$. Therefore, the cold gas content of late type galaxies corresponds to about 20% of the stellar mass content and about 2% of the total baryonic content in the universe.

The authors acknowledge insightful discussions with N. Katz, M. Heyer, S. Hüttemeister, and others. Comments by our referee, Martin Zwaan, were quite helpful for improving the manuscript. This research has made use of the NASA/IPAC Extragalactic Database (NED) which is operated by the Jet Propulsion Laboratory, California Institute of Technology, under contract with the National Aeronautics and Space Administration. D. Keres gratefully acknowledge the partial research support provided by the Mary Dailey Irvine graduate research fellowship. The Five College Radio Astronomy Observatory is operated with the permission of the Metropolitan District Commission, Commonwealth of Massachusetts, and with the support of the National Science Foundation under grant AST 97-25951.

REFERENCES

- Benson, A. J., Frenk, C. S., & Sharples, R. M. 2002, ApJ, 574, 104
 Bloemen, J. B. G. M., et al. 1986, A&A, 154, 25
 Briggs, F. H., & Rao, S. 1993, ApJ, 417, 494
 Burles, S., Nollett, K. M., Turner, M. S. 2001, ApJ, 552, L1
 Casoli, E. et al. 1998, A&A, 331, 451
 Cole, S., et al. 2001, MNRAS, 326, 255
 Condon, J. J. 1987, ApJS, 65, 485
 Condon, J. J., Anderson, M. L., & Helou, G. 1991, ApJ, 376, 95
 Condon, J. J., Cotton, W. D., Broderick, J. J. 2002, AJ, 124, 675
 de Bernardis, P. et al. 2002, ApJ, 564, 559
 de Vaucouleurs, G., de Vaucouleurs, A., Corwin, H. 1976, Second Reference Catalogue of Bright Galaxies (Austin: Univ. of Texas Press) (RC2)
 Devereux, N., Young, J. S. 1990, ApJ, 359, 42
 Dickman, R. L., Snell, R. L., & Schloerb, F. P. 1986, ApJ, 309, 326
 Downes, D., Solomon, P. M. 1998, ApJ, 507, 615
 Fukugita, M., Hogan C. J., Peebles, P. J. E. 1998, ApJ, 503, 518
 Helou, G., Khan, I. R., Malek, L., Boehmer, L. 1988, ApJS, 68, 151
 Hibbard, J. E., Yun, M. S. 1996, "The Neutral Hydrogen Distribution in Luminous Infrared Galaxies" in the "Cold Gas at High Redshifts" eds. M. N. Bremer, P. P. van der Werf, H. J. A. Rottgering, C. L. Carilli, p.47
 Kenney, J. D. P., & Young, J. S. 1988, ApJS, 66, 261
 Kenney, J. D. P., & Young J. S., 1989, ApJ, 344, 171
 Maloney, P., & Black, J. H. 1988, ApJ, 325, 389
 Marzke, R. O., Huchra, J. P., Geller, M. J. 1994, ApJ, 428, 43
 Paglione, T. A. D., et. al 2001, ApJS, 135, 183
 Perea, J., del Olmo, A., Verdes-Montenegro, L. & Yun, M. S., ApJ, 490, 166
 Press, W. H., & Schechter, P. 1974, ApJ, 187, 425
 Rao, S., Briggs, F. H. 1993, ApJ, 419, 515
 Rice, W., et. al 1988, ApJS, 68, 91
 Sakamoto, K., Okumura, S. K., Ishizuki, S., Scoville, N. Z. 1999, ApJ, 525, 691
 Sage, L.J. 1993, A&A, 272, 123
 Sage, L. J., Wrobel, J. M. 1989, ApJ, 344, 204
 Sandage, A., Tammann, G. A. 1981, A Revised Shapley-Ames Catalog of Bright Galaxies (Washington, DC: Carnegie Institution of Washington) (RSA)
 Sanders, D. B., Scoville, N. Z., Soifer, B. T. 1991, ApJ, 370, 158
 Sanders, D. B., Egami, E., Lipari, S., Mirabel, I. F., & Soifer, B. T. 1995, AJ, 110, 1993 (BGS2)
 Schechter, P. 1976, ApJ, 203, 297
 Schmidt, M. 1968, ApJ, 151, 393
 Schneider, S. E., Spitzak, J. G., Rosenberg, J. L. 1998, ApJL, 507, L9
 Scoville, N. Z., Sanders D. B. 1987, In *Interstellar Processes*, ed. D. Hollenbach, H. Thronson, p. 21. Dordrecht, Reidel
 Scoville, N. Z., Yun, M. S., & Bryant, P. M. 1997, ApJ, 484, 701
 Soifer, B. T., et al. 1987, ApJ, 320, 238
 Soifer, B. T., Boehmer, L., Neugebauer, G., and Sanders, D. B. 1989, AJ, 98, 766 (BGS1)
 Solomon, P. M., Sage, L. 1988, ApJ, 334, 613
 Tully, R. B. 1988, Nearby Galaxies Catalog, (Cambridge: Cambridge Univ. Press)
 Verter, F. 1987, ApJS, 65, 555
 Wilson, C. D. 1995 ApJL, 448, L97
 Young, J. S., Xie, S., Kenney, J., Rice, W. L. 1989, ApJS 70, 699
 Young, J. S., Knezek, P., 1989, ApJL 347, L55
 Young, J. S., Scoville, N. Z., 1991, ARAA, 29, 581
 Young, J. S., et al. 1995, ApJS, 98, 219
 Young, J. S., et al. 2002, in preparation
 Yun, M. S., Reddy, N. A., & Condon, J. J. 2001, ApJ, 554, 803
 Zwaan, M. A., Briggs, F. H., Sprayberry, D., & Sorar, E. 1997, ApJ, 490, 173

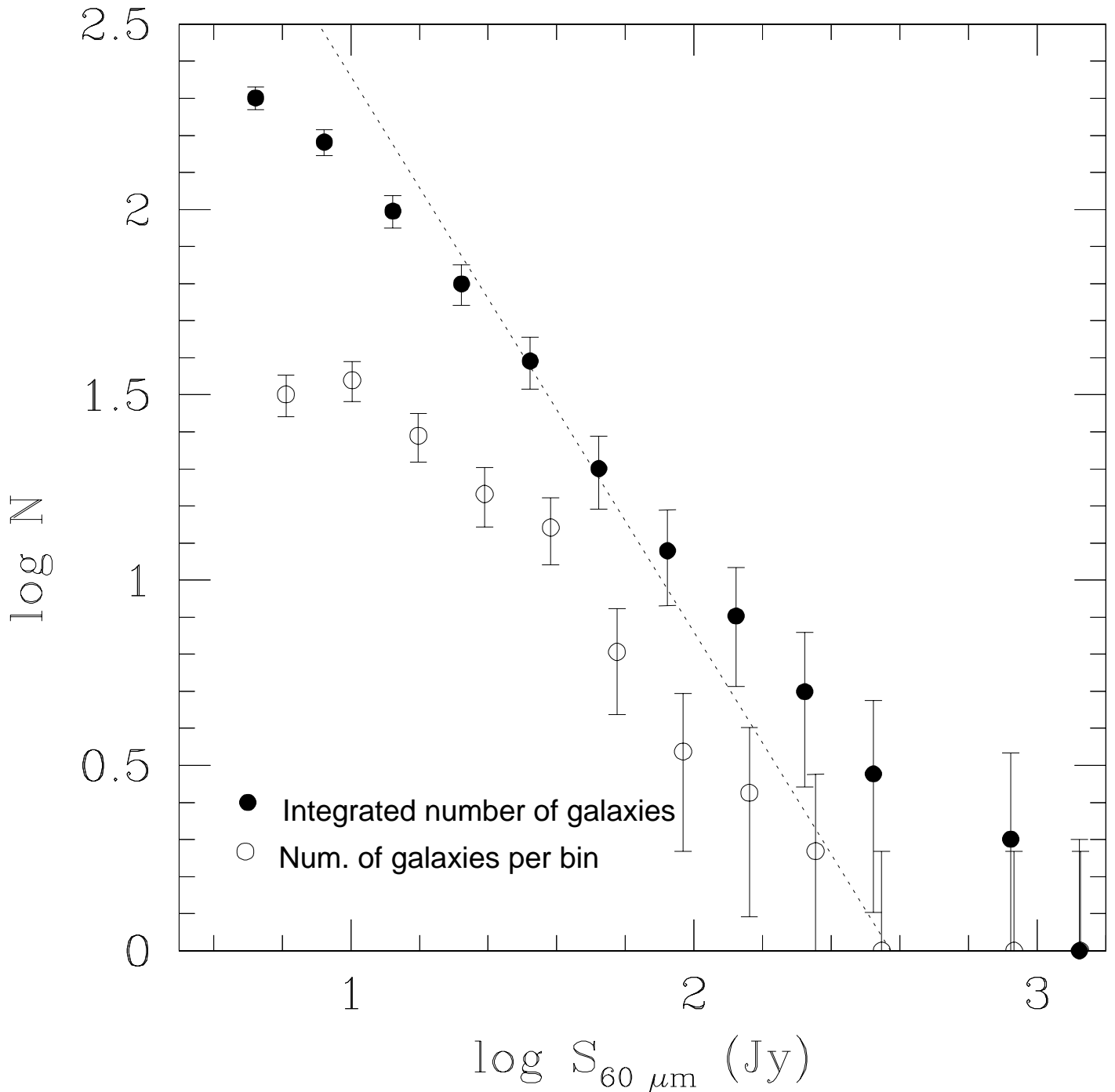


FIG. 1.— Number of galaxies per bin (0.2 in log scale) of $60 \mu\text{m}$ flux density and integrated number of galaxies. Although the number of galaxies per bin grows with decreasing flux density, the power-law slope of $\alpha \sim -1$ suggests a non-uniform distribution of sources. The dotted line represents the expected behavior of uniformly distributed non-evolving sources in Euclidean geometry, appropriate for the 601 galaxies in the two BGS samples. The fact that high flux bins are higher than the complete sample line is noticed also in BGS (Soifer et al. 1989) and is caused by large scale structures. The lowest luminosity bins are lower than expected probably because sources near the flux cutoff that are spatially resolved by IRAS have systematically lower flux entries in the Point Source Catalog and are thus missed.

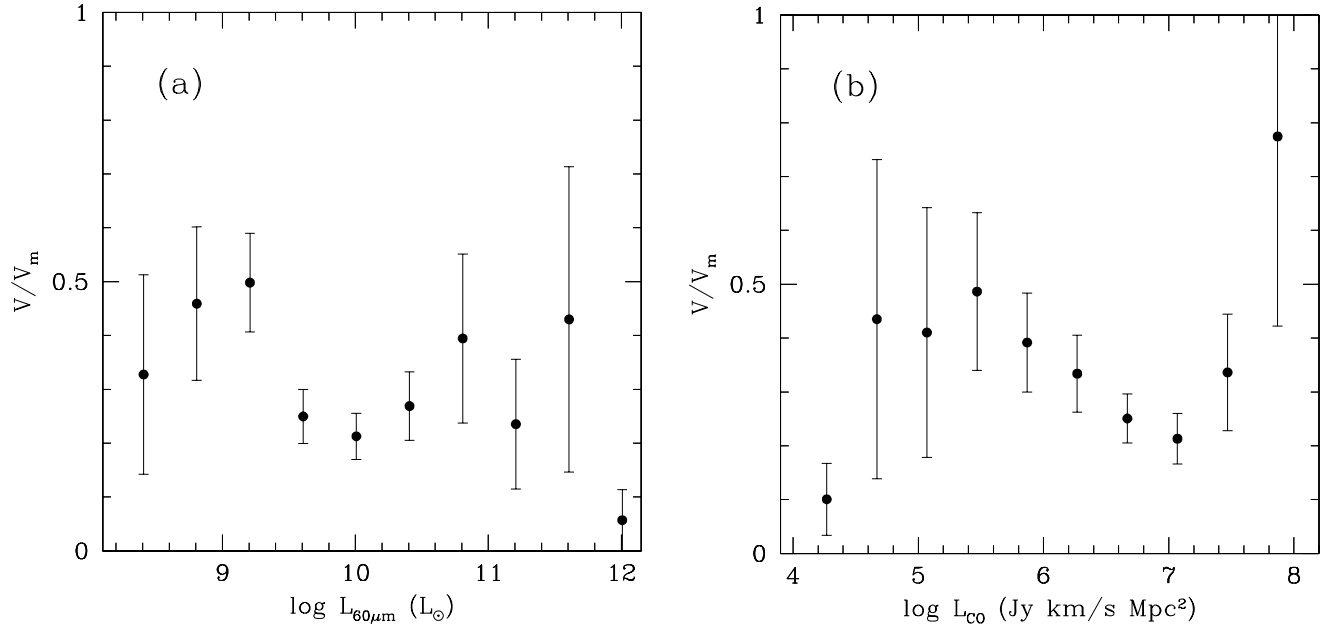


FIG. 2.— V/V_m analysis for (a) the $60\ \mu\text{m}$ LF and (b) the CO LF. The mean value of $V/V_m \sim 0.35$ suggests that our sample galaxies are on average about 10% closer than the uniform case.

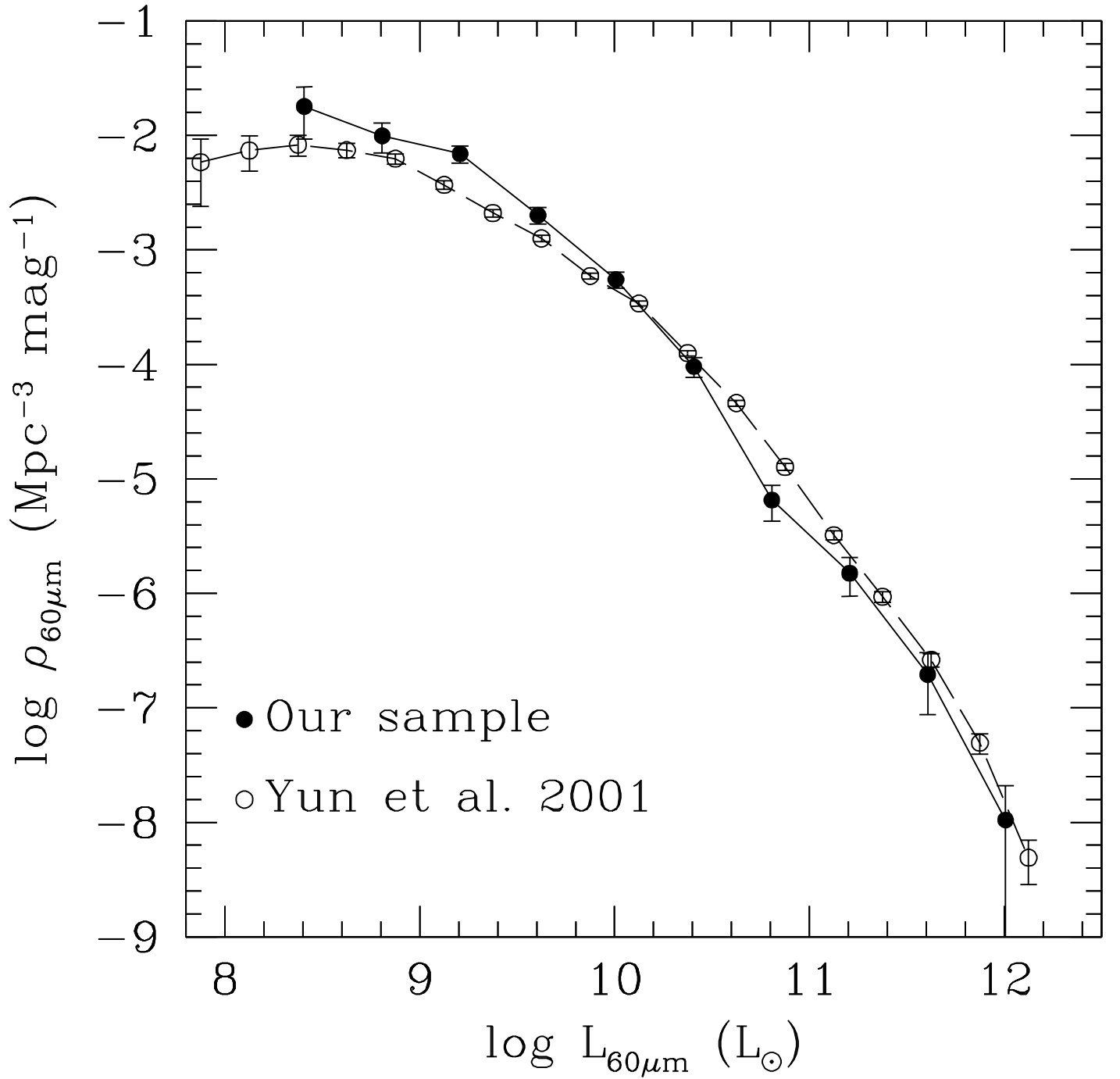


FIG. 3.— IRAS 60 μm LF obtained using our CO sample of 200 galaxies corrected for the sample selection. The comparison with the 60 μm LF derived from a much larger sample obtained by Yun et al. (2001) shows a good agreement.

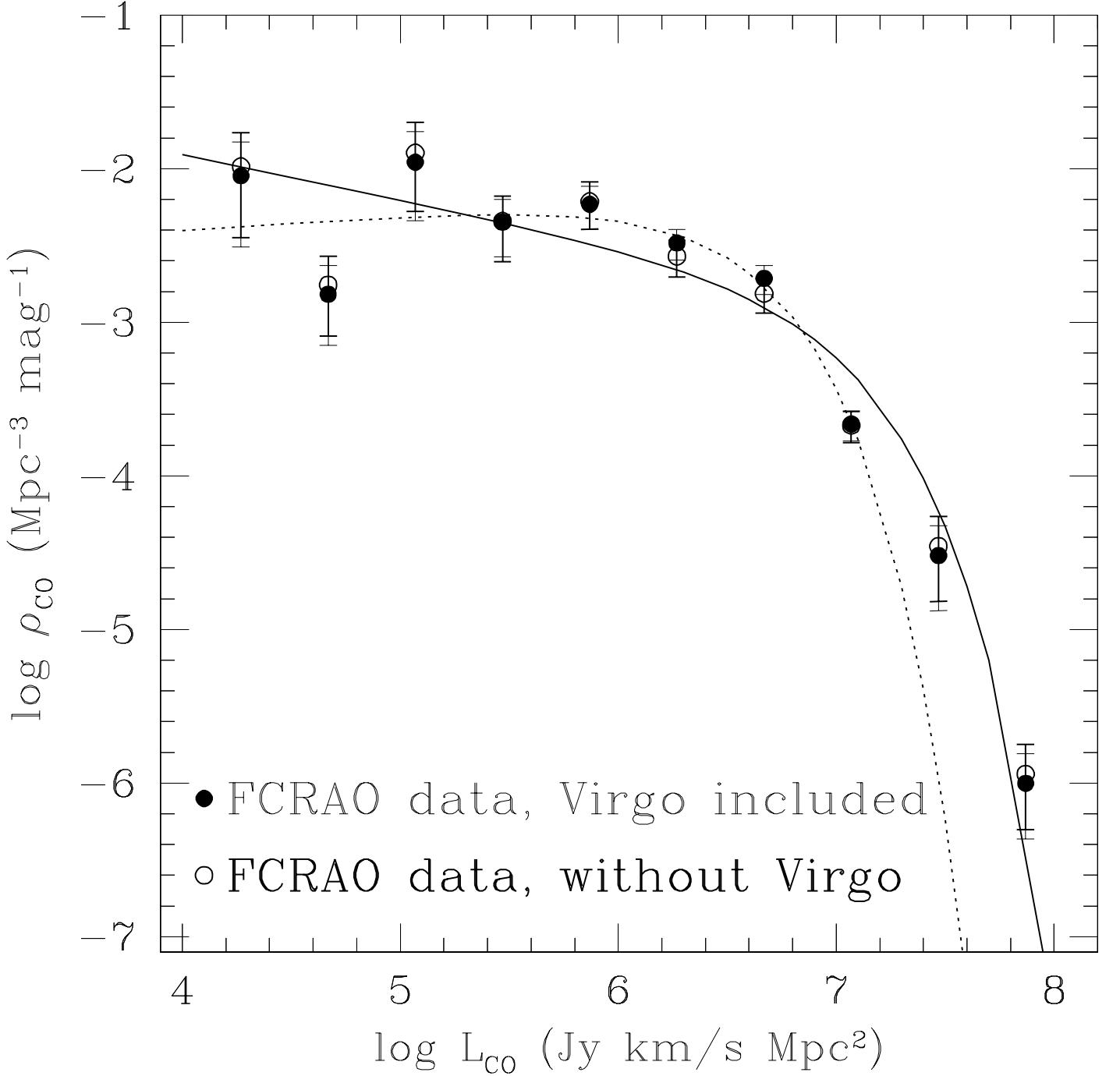


FIG. 4.— The CO luminosity function, derived using the same sample and volume correction as the IRAS $60 \mu\text{m}$ LF shown in Figure 3. The solid line is the best fit Schechter function derived using all 10 bins. The CO LF follows a Schechter function shape closely with a faint end power-law index $\alpha = -1.30$ and the characteristic luminosity $L^* = 9.8 \times 10^6 \text{ Jy km s}^{-1} \text{ Mpc}^2$. The dotted line shows the best fit Schechter function derived excluding the two highest luminosity bins (see § 3.2). The power-law index for this fit is $\alpha = -0.90$ and $L^* = 3.3 \times 10^6 \text{ Jy km s}^{-1} \text{ Mpc}^2$.

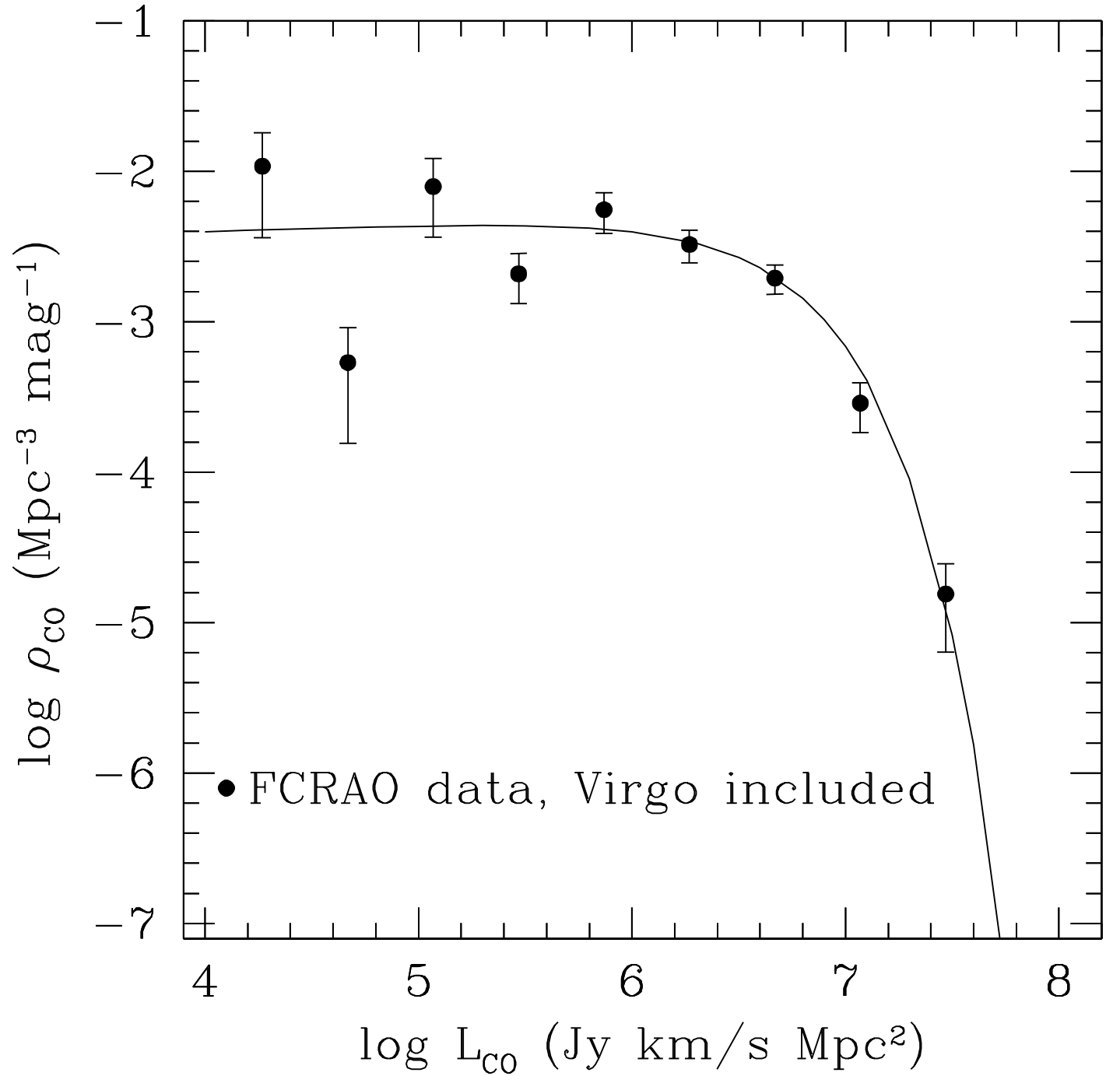


FIG. 5.— The CO luminosity function obtained for the optical B -band selected sample derived from the RSA catalog as the parent sample. The solid line shows the best fit Schechter function (see text).

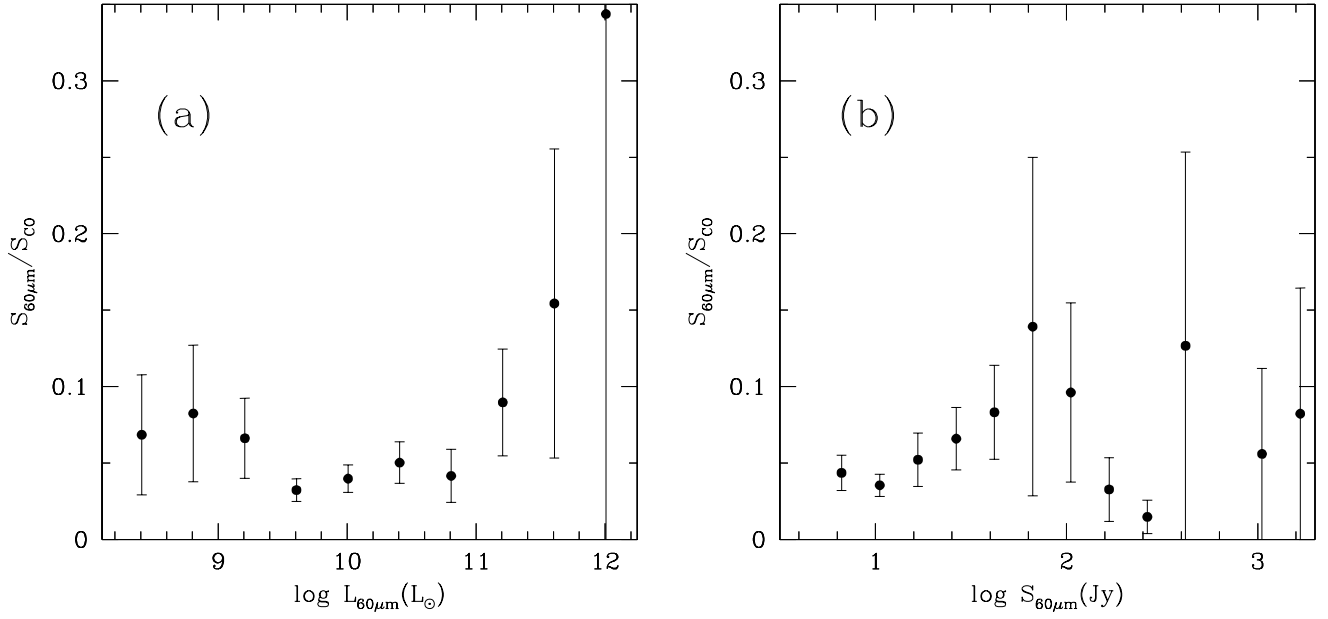


FIG. 6.— (a) Average $S_{60\mu m}/S_{CO}$ vs. $L_{60\mu m}$. High luminosity bins have higher values of $S_{60\mu m}/S_{CO}$, but they also suffer from the small number statistics. (b) Average $S_{60\mu m}/S_{CO}$ vs. $S_{60\mu m}$. The absence of any clear trend in either plots suggests that our IRAS selection does not introduce any obvious bias to the CO measurements.

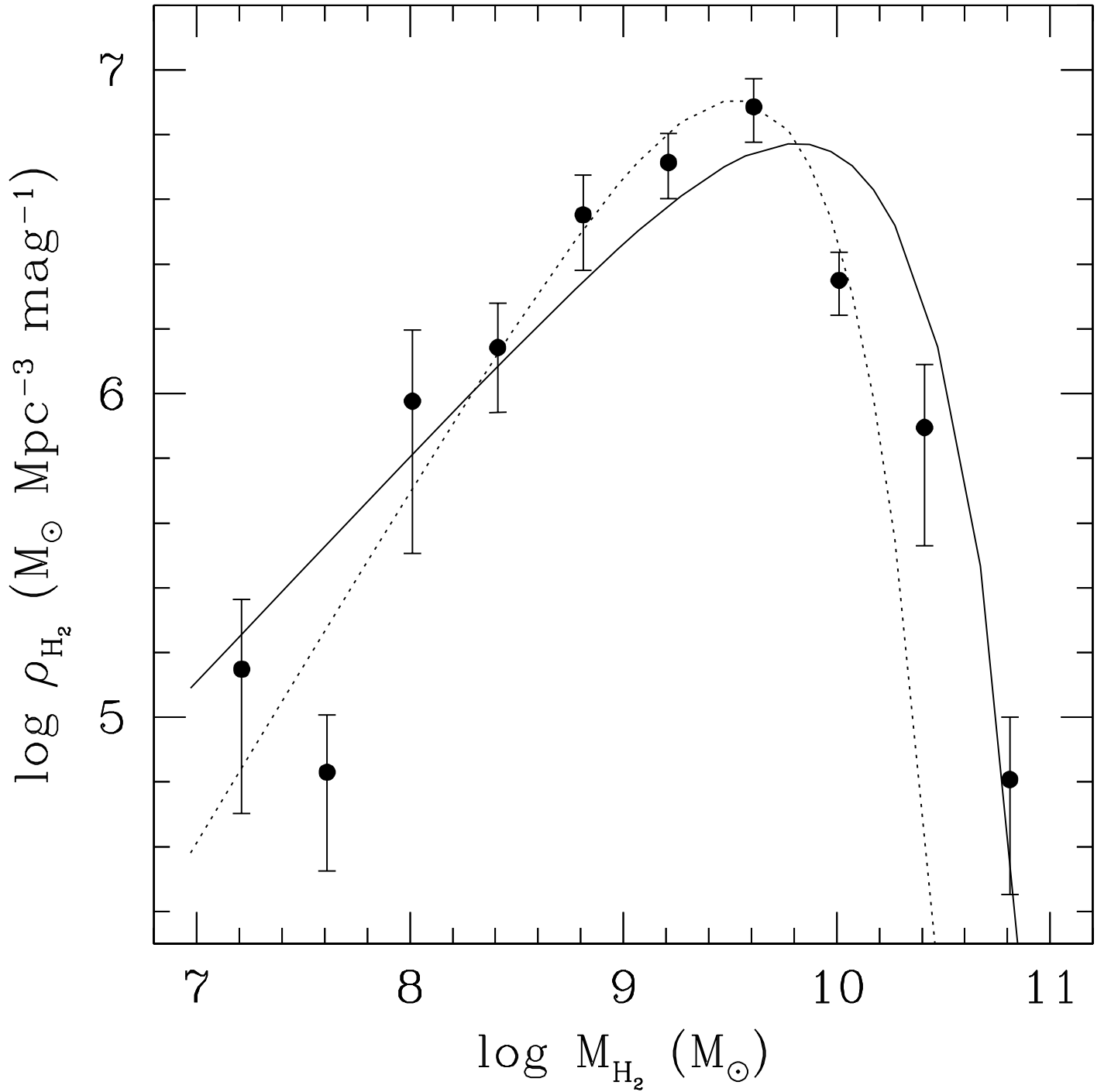


FIG. 7.— Molecular mass density contribution per magnitude of H_2 mass. The H_2 mass bins near the M^* value, $\log M_{H_2} \sim 9.5$, dominate the contribution to the total mass density. The solid and dotted lines correspond to the same lines shown in Figure 4.

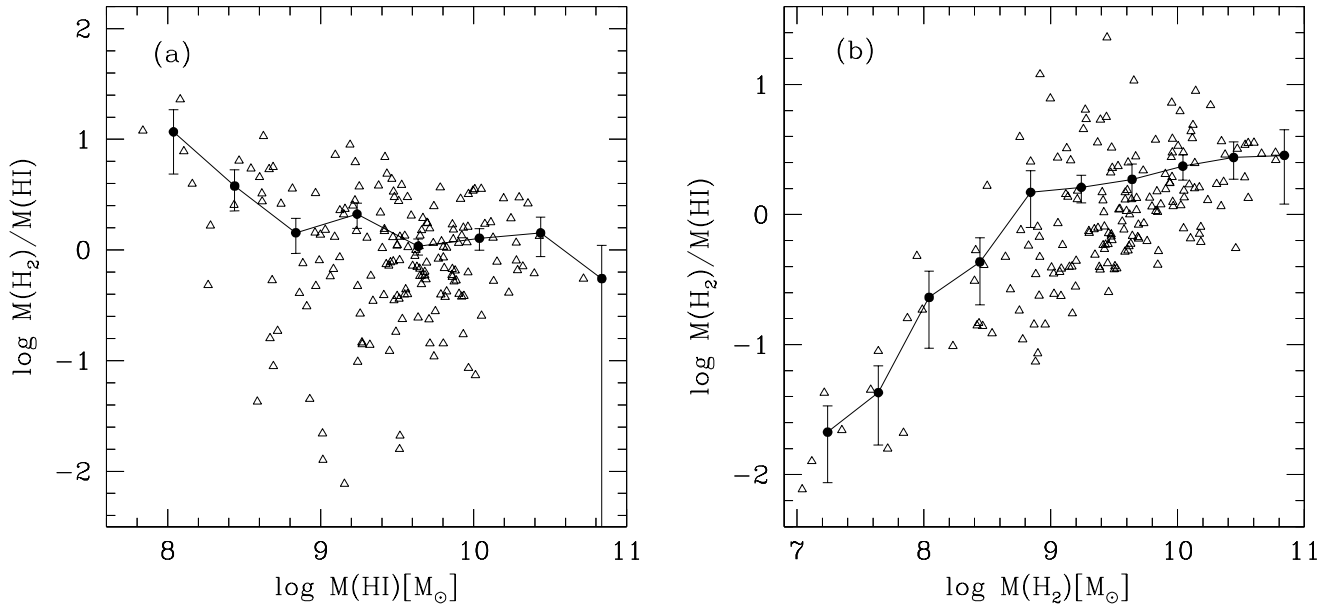


FIG. 8.— The molecular to atomic hydrogen mass ratio are shown as a function of (a) M_{HI} and (b) M_{H_2} . Individual galaxies are shown as triangles while the bin averages are shown with filled circles and connected in solid lines to accentuate the trend of growing $M(H_2)/M(HI)$ ratio for larger H_2 masses.

TABLE 1
GALAXIES WITH $S_{60} > 5.24$ JY NOT DETECTED IN THE SURVEY

Name	R.A. [h m s]	dec [d m s]	D [Mpc]	S_{60} [Jy]	S_{CO} [Jy km/s]	Type	Ref.
NGC 337	00 59 50.3	-07 34 44	23.7	9.33	140	Sd	u
NGC 470	01 19 44.8	+03 24 35	35.6	7.09	180	Sb	u
NGC 693	01 50 31.0	+06 08 42	21.9	6.86	70	S0/a	u
NGC 925	02 27 17.0	+33 34 43	9.5	9.03	566	Sd	1
NGC 3227	10 23 30.6	+19 51 54	20.6	8.32	756	SAB (pec)	*
NGC 3486	11 00 23.9	+28 58 30	7.4	6.24	263	Sc	1
NGC 4027	11 59 28.4	-19 19 55	19.5	11.89	60	Sdm	u
NGC 4526	12 34 03.1	+07 41 59	16.0	5.63	87	S0	2
NGC 4532	12 34 19.3	+06 28 07	16.0	8.93	60	Im	u
NGC 4808	12 55 48.9	+04 18 13	16.0	6.92	100	Scd	u
NGC 6824	19 43 40.9	+56 06 33	49.0	5.94	30	Sb	u
Mrk 273	13 44 47.5	+55 54 11	153.8	22.09	62	Merg.	3

Coordinates are for J2000 and are taken from NASA Extragalactic Database. S_{60} is IRAS 60 μ m flux density taken from BGS1 and BGS2 except for NGC 925 where we used value from Rice et. al (1988) increased by 18%. References for S_{CO} (column 8) are: 1.-Sage (1993); 2.-Sage & Wrobel (1989); 3.-Sanders et. al (1991); u - upper limit from Young et al. (1995). *-a new measurement of central 45'' obtained using the FCRAO 14-m telescope in March 2002. NGC 3227 was not included in the Survey originally because this galaxy was confused with NGC 3226.